Aerospace Science and Technology 73 (2018) 300–308

Contents lists available at ScienceDirect

Aerospace Science and Technology

www.elsevier.com/locate/aescte

Broadband reduction of the specular reflections by using sonic crystals: A proof of concept for noise mitigation in aerospace applications

L.M. Garcia-Raffi [a], L.J. Salmerón-Contreras [a], I. Herrero-Durá [b], R. Picó [b,*], J. Redondo [b], V.J. Sánchez-Morcillo [b], K. Staliunas [c], N.J.E. Adkins [d], A. Cebrecos [e], N. Jiménez [f], V. Romero-García [e]

[a] Instituto Universitario de Matemática Pura y Aplicada, Universitat Politècnica de València, València, Spain
[b] Instituto de Investigación para la Gestión Integrada de Zonas Costeras, Universitat Politècnica de València, València, Spain
[c] Institució catalana de Recerca i Estudis Avançats (ICREA), Barcelona, Spain
[d] Dept. of Metallurgy and Materials, The University of Birmingham, Edgbaston, Birmingham, B15 2TT, United Kingdom
[e] Laboratoire d'Acoustique de l'Université du Maine (LAUM) - CNRS UMR 6613, Av. Olivier Messiaen, 72085, Le Mans, France
[f] Instituto de Instrumentación para Imagen Molecular (I3M), Centro Mixto Universitat Politècnica de València CSIC CIEMAT, Camino de Vera s/n, 46022 Valencia, Spain

ARTICLE INFO

Article history:
Received 8 June 2017
Received in revised form 10 October 2017
Accepted 30 November 2017
Available online 8 December 2017

Keywords:
Sonic crystals
Noise reduction
Diffusion
Insertion loss
Reflection

ABSTRACT

The broadband reduction of the specular reflections by sonic crystals (SCs) is theoretically and experimentally reported in this work. The analysed system consists of a sound source radiating a SC made of acoustically rigid scatterers embedded in water partially covering an open cavity. By comparison with a reference flat reflector, we observe that reflected waves spread in space as a consequence of the spatially modulated properties of the SC. Moreover, due to the different working frequency ranges of the SC a significant noise reduction is produced in a broadband region. Therefore, due to the spreading of the reflected waves, the system produces a broadband noise reduction in the area of the source. In particular, the noise reduction is close to 2 dB for the two octaves emitted by our source, which represents a decrease of 37% of the acoustic energy. The results shown in this work constitute a proof of concept for the use of SCs as broadband-noise reduction systems at the launch pad. An approach to the geometry of the Vega launch vehicle the European Space Agency is proposed and the limitations of the study are discussed.

1. Introduction

Sonic crystals (SCs) are artificial structures made of periodic arrangements of solid scatterers embedded in a host fluid medium. The materials constituting the scatterers and the fluid host present high contrast in their physical properties (i.e., in density, ρ, and sound velocity, c) [1]. Usually SCs are made of solid cylinders of metal [2], plastic [3] or wood [4] embedded in a fluid (usually air [5] or water [6]). The dispersion relation of such systems has been dramatically exploited during the last years to control acoustic waves for several purposes, as for example noise reduction [7], waveguiding [4], focusing [8], collimating [9,10] or localizing [11] waves. Perhaps, the most known property of SCs is the presence of band gaps, ranges of frequencies in which the propagation of waves is evanescent due to the destructive interference produced by the Bragg reflections. Fig. 1 shows the dispersion relation of a small-scale additively manufactured SC with square periodicity in two dimensions (shown in the inset) when it is embedded in water ($\rho_{host} = 1000$ kg/m^3, $c_{host} = 1450$ m/s). Red regions represent the directional band gaps of the structure, appearing around the Bragg's frequency, $fa/c_{host} = 1/2$ (a being the lattice constant of the SC, i.e., the distance between the centre of the rods).

Reflection of waves by this kind of structures is, in general, non-specular and produces diffusiveness of the sound field. Particularly, SCs of finite dimensions have been shown as efficient sound diffusers not only in the high frequency range, but also at low frequencies, by means of different mechanisms, mixing both periodic and finite size effects [12]. SCs also improve the diffusion when compared to other structures proposed in the literature (being the Schroeder diffuser [13] the paradigmatic example), in particular at low frequencies.

In this work, we experimentally and theoretically report the broadband reduction of the amplitude of specular reflections by using a SC made of metal scatterers embedded in water. The anal-

* Corresponding author.
E-mail address: rpico@fis.upv.es (R. Picó).

https://doi.org/10.1016/j.ast.2017.11.048
1270-9638/

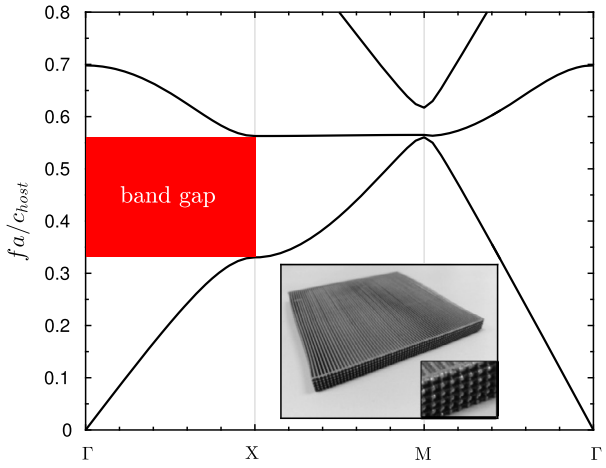

Fig. 1. Dispersion relation of the small-scale additively manufactured SC with square periodicity (shown in the inset) when it is embedded in water ($\rho_{host} = 1000$ kg/m^3, $c_{host} = 1450$ m/s). The range of frequencies are normalized, fa/c_{host}, by the lattice constant of the SC and by the sound velocity of the host medium, in this case water. Red region shows the band gap at the ΓX direction, i.e., along the normal incident direction. (For interpretation of the references to colour in this figure, the reader is referred to the web version of this article.)

ysed system consists of an acoustic source that radiates waves into a SC placed over an open cavity. By comparison with a reference flat reflector, we observe that the reflected waves spread in space as a consequence of the spatially modulated properties of the SC. Moreover, as the SC works in a large range of frequencies, the noise reduction is broadband. Therefore, due to the spreading of reflected waves, the system produces a broadband noise reduction in the area between the source and the SC.

The results of this study constitute a proof of concept in which the main motivation is to incorporate SCs in future launch-pad designs as a broadband noise reduction system for aerospace applications [14]. Recent studies show the relevance of noise reduction in the launch pad during the lift-off of launch vehicles, since it is predicted to improve both the reliability and the operations of future launchers [15–19]. In fact, the acoustic loads experienced by the launch vehicle occur with strong interaction between the rocket and the launch facility, putting at risk the missions with potentially high economic cost. Thus, the reduction of the acoustic levels in the vicinity of the launch vehicle is an important factor that should be taken into consideration early in the design of the launch site. The results shown in this work are a first proof of concept for the use of SCs as broadband-noise reduction systems at the launch pad. Our proposal, unlike other recent alternatives [20,21], does not exclude the use of other noise reduction mechanisms as water deluge.

The work is organized as follows. In Section 2 we define the problem analysed in this work as well as the parameters used for the characterization of the physical properties of the structure. In Section 3 we present the diffusion produced by a single SC in order to introduce the concept of diffusion as well as the different working regimes of the SCs. In Section 4 we describe the experimental setup and the different SCs experimentally tested. Experimental data of the system are presented in Section 5, showing the results of the diffusion coefficient as well as the reduction of the reflected field near the SCs. In Section 6 the application of SCs as a noise reduction system in future launch pads is introduced, discussing the real-scale geometry and SCs proposed for the Vega launch site of the European Space Agency [22], as well as the limitations of the scale-model. Finally, Section 7 summarizes the conclusions of the work.

2. Definition of the problem

2.1. The geometry

The structure under analysis in this work is made of two main elements as shown in Fig. 2(a): (*i*) the SC (in blue) and (*ii*) the cavity, that is, the air volume confined between the SC and a rigid backing (in grey). The SC is made of an arrangement of $n \times m$ square rod scatterers of side length l (n is the number of columns and m the number of rows of the SC). The scatterers are considered acoustically rigid (high contrast between the mechanical properties of the host and the scatterers) and they are placed by following a square array which lattice constant is a (see also in Fig. 2(a) the unit cell). Therefore, the filling fraction is defined as $F = l^2/a^2$. The length h determines the distance between the bottom of the cavity and the last row of the SC.

In this work we will consider the case of linear propagation (small amplitude propagation). At this stage it is worth noting here that, if the host fluid is chosen with the proper viscosity, the problem is fully scalable, and the results can be normalized with respect to the characteristic scale of the system (lattice constant, a) and with respect to the host medium properties (sound velocity, c_{host}). Then, the frequencies can be also normalized using fa/c_{host}, where f is the frequency. Thus, a scale-model in water and in the ultrasonic regime is proposed for the experimental measurements. The real-scale dimensions in air and in the audible sound regime are given in Section 6. Note we selected water as the host fluid to maintain constant the ratio between the viscous boundary layer and the lattice step in both situations. See Section 6 for further details.

2.2. Definition of parameters

We use two parameters to evaluate the diffusion of sound by the analysed structures: the diffusion coefficient and the Insertion Loss (IL). The first one is a single index which gauges the uniformity of the polar response. The second one measures the noise reduction level in the near field area.

2.2.1. Diffusion coefficient

The diffusion coefficient, δ, is derived from the polar scattered field. If the polar response is evaluated at n points equally spaced over test specimen, the diffusion coefficient is calculated as [13]

$$\delta = \frac{\left(\sum_{i=1}^{n} I_i\right)^2 - \sum_{i=1}^{n} I_i^2}{(n-1)\sum_{i=1}^{n} I_i^2}, \tag{1}$$

where I_i is the sound intensity of the reflected sound at the i-th polar location. The diffusion coefficient is bounded, ranging from $\delta = 0$ (the sample scatters all acoustic energy only in one direction) to $\delta = 1$ (waves are scattered in every direction with the same amplitude).

The normalized diffusion coefficient, δ_n, is evaluated as

$$\delta_n = \frac{\delta - \delta_{\text{ref}}}{1 - \delta_{\text{ref}}}, \tag{2}$$

where δ and δ_{ref} are respectively the diffusion coefficients for the test structure, i.e., the SC, and for a reference flat reflector of the same overall size than the SC, respectively, both calculated using Eq. (1). The normalized diffusion coefficient δ_n gives the diffusion coefficient of the structure showing the differences with respect to a perfectly-reflecting flat reflector: when $\delta_n = 0$, the whole structure behaves like the reference flat reflector, and when $\delta_n > 0$ ($\delta_n < 0$), it has a bigger (smaller) coefficient diffusion than that of the reference flat reflector.

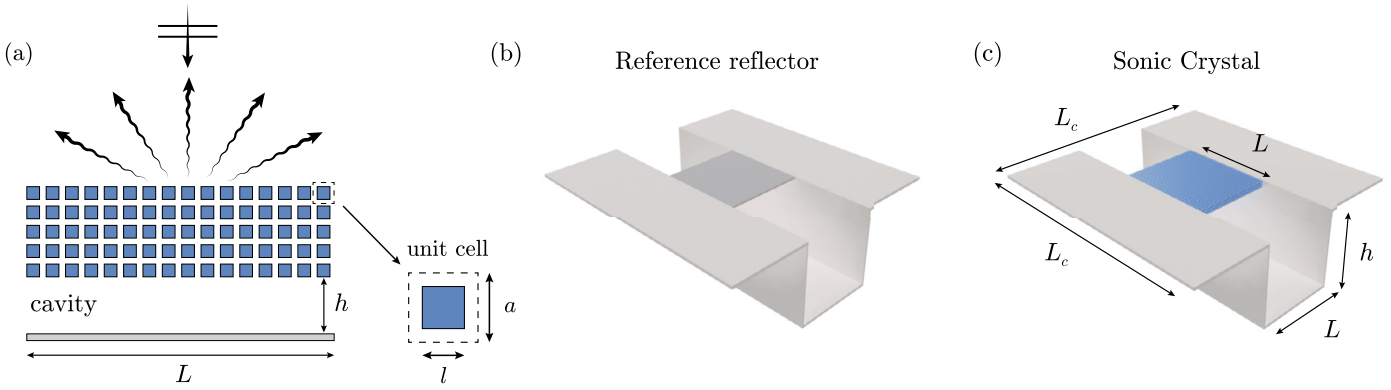

Fig. 2. (a) Definition of the problem: a plane wave impinging the structure made of a SC placed a distance h over a flat rigid backing. The transversal length of the system is L, in such a way that $L = n \times a$, where n is the number of columns in the SC and a is the lattice constant, i.e. the distance between scatterers. The scatterers are square rods of side length l. (b) Configuration used as a reference by changing the SC by a rigid flat reflector. (c) SC placed in a rigidly-backed cavity.

2.2.2. Insertion loss

A common method used to characterize linear systems in many fields is the *IL*. A general definition is the loss of signal power resulting from the insertion of a device in a transmission line. In the context of acoustics, the *IL* is defined as the difference in sound pressure levels measured before and after a barrier or silencer installed in the line between the source and the receiver [3]. This magnitude represents the attenuation provided by the insertion of a structure between the noise source and the receiver, and it is an estimation of reduction of the transmitted acoustic energy.

In the problem considered here, the noise source is located at the same side as the receiver. The *IL* of a structure following this configuration indicates the reduction of the reflected energy. We aim to characterize the difference in the pressure field in the region between the noise source and the SCs. As a consequence, we propose to use a natural extension of the original definition of the *IL*, but here in reflection. In order to evaluate the efficiency for sound mitigation of a SC, the *IL* in reflection is calculated as the difference (in dB) between the total sound pressure level measured in a reference situation, P_{ref}, as shown in Fig. 2(b), with respect to the total sound pressure level measured when the SC has been placed at the same position, P_{SC}, as shown in Fig. 2(c), which is given by

$$IL\,[\text{dB}] = 10 \log_{10} \frac{|P_{\text{ref}}|^2}{|P_{\text{SC}}|^2} = L_{\text{ref}} - L_{\text{SC}}, \tag{3}$$

where L_{ref} and L_{SC} are the sound pressure levels of the reference flat reflector and the SC respectively. It is assumed that the incident field emitted by the source in both configurations is identical. As we will emphasize later, the *IL* is a function of both, frequency and space, and we will present results considering the integration with respect to each of these two variables.

3. Sound diffusion by sonic crystals: from surface to bulk effects

We start analysing numerically the diffusion coefficient of a single SC. The numerical results are obtained by solving the acoustic wave equation assuming harmonic time-dependence using the Finite Element Method (FEM), which is applied for a two-dimensional case. The spatial domain is surrounded by Perfectly Matched Layers (PML). The scatterers are assumed acoustically rigid (infinite impedance), corresponding to Neumann boundary conditions at the interface with the fluid. The incident field was generated by a plane wave travelling towards the SC at normal incidence. The scattered far-field is calculated in a semi-circumference of radius R centred in the sample and using the far-field transformation [13]. In this section we study only the presence of the crystal, without the cavity. The interest of this section is to show the effects of the crystal itself on the diffusion coefficient. We will investigate the dependence of the normalized diffusion coefficient, δ_n, for several configurations made from $m = 1$ to $m = 5$ rows in a square lattice crystal of $n = 17$ columns, as shown schematically in Fig. 2(a). The SC is characterized by a filling fraction of $F = 0.49$.

Figs. 3(a)–(e) show the scattered far-fields for the structures made of $m = 1$ to $m = 5$ rows, respectively, being the width equal to $n = 17$ columns in all cases. In comparison with the diffusion of a reference flat reflector, the SC introduces a complex scattered field, which as we will see, increases the diffusion coefficient of the system. We observe that the scattered field has a component along the incident direction, 0°, which gives the specular behaviour of the structure. Non-specular components emerge along other directions which are the result of the reflection of waves due to two effects: the periodicity and finite size of the SC. In fact, there is a combination of the periodicity in the surface (interface SC-surrounding medium), the periodicity in the bulk of the SC, and the finite size of the crystal. The first one, produces the high order diffraction modes, due to the diffraction grating character of the surface [23], which are represented in the scattered far-field by the branches at angles different than the specular one. The second one, produces the modulation of the field along these branches, at frequencies related with the periodicity. The third one, introduces modulation of the scattered field at low frequencies.

In order to see all of these effects, we study the normalized diffusion coefficient for each structure. Fig. 3(f) shows the normalizes diffusion coefficient δ_n for each structure. Black, red, blue, dashed red and dashed blue lines represent the d_n for the structures made of 17×1, 17×2, 17×3, 17×4 and 17×5 scatterers, respectively. First of all, we notice that δ_n is bigger than 0 for the whole range of frequencies, so the diffusion produced by the SC is bigger than that of a flat rigid surface. In addition, we can differentiate three ranges of frequencies (marked with arrows in Fig. 3(f)) where the diffusion coefficient is highly increased with respect to a reference flat reflector. We see an increase at low frequencies (normalized frequencies lower than 0.25), other around the region of $fa/c_{host} = 0.6$ and finally another one around $fa/c_{host} = 1$.

At low frequencies, we see that the peaks of diffusion highly depend on the number of rows in the structure. To explain these peaks we need to consider the crystal as an equivalent fluid characterized by [24]

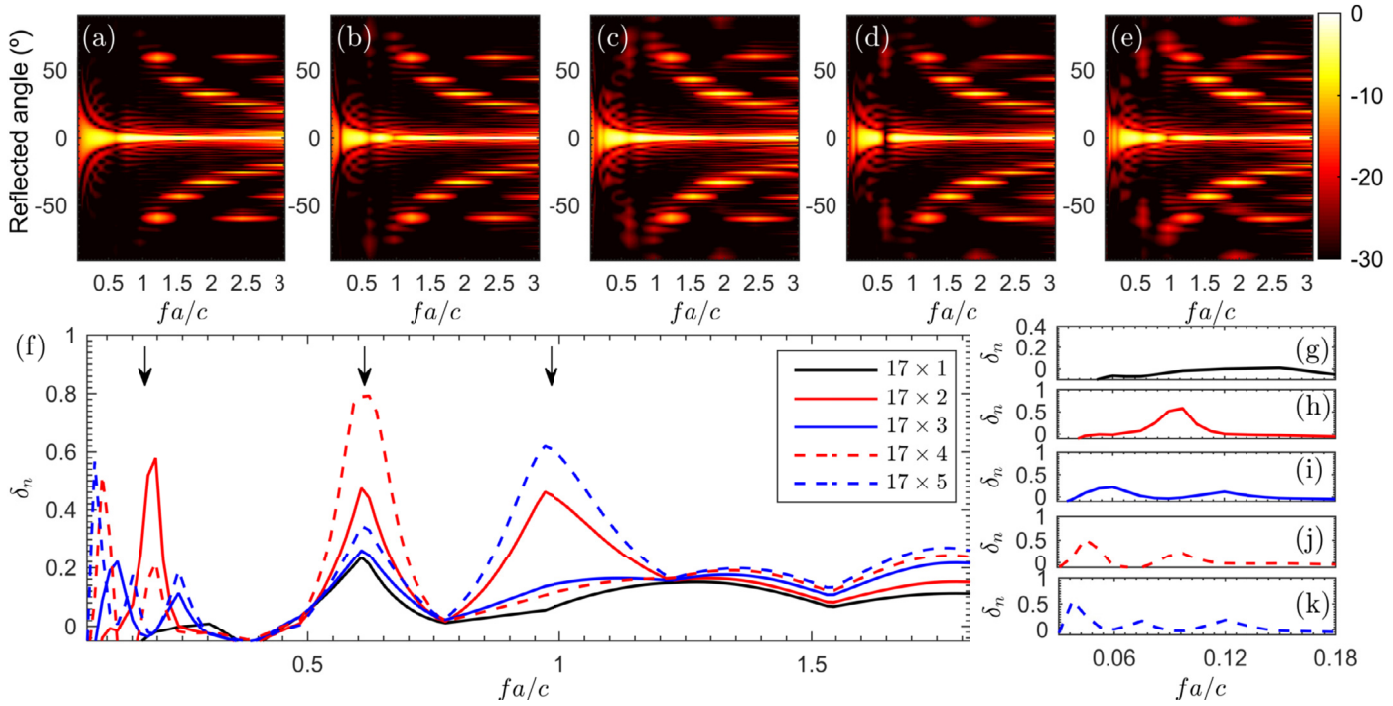

Fig. 3. Scattering by a SC structure with a $F = 0.49$. (a)–(e) Show the scattered far-field for the structures made of $m = 1$ to $m = 5$ rows respectively, with $n = 17$. (f) Shows the normalized diffusion coefficients for the five structures, arrows show the effects of the Fabry–Pérot (low frequencies), periodicity (medium frequencies) and diffraction order (high frequencies). Black, red, blue, dashed red and dashed blue lines represent the δ_n for the structures made of 17×1, 17×2, 17×3, 17×4 and 17×5 scatterers respectively. (g)–(k) Show the zoom in the low frequency regime for the case from 1 to 5 rows respectively to analyse the Fabry–Pérot resonances. (For interpretation of the references to colour in this figure, the reader is referred to the web version of this article.)

$$c_{eff} = c_{host} \frac{1}{\sqrt{1+F}}, \tag{4}$$

$$\rho_{eff} = \rho_{host} \frac{1+F}{1-F}. \tag{5}$$

c_{eff} and ρ_{eff} are the effective velocity and density of the crystal in the range of frequencies lower than $fa/c_{host} = 0.25$ (low frequency regime or also homogenization regime [24]). If we consider the system made by m rows, the crystal behaves like a slab of width ma, then considering the sound velocity c_{eff} one can predict $m-1$ resonances, known as Fabry–Pérot (FP) resonances, due to the finite width of the crystal, given by $f_r = c_{eff}/(2ma)$. For one row, the resonance peak is out of the range of homogenization, so we do not predict any peak as shown in Fig. 3(g). For the rest of the structures (from 2 to 5 rows) we can predict different resonances depending on the width of the structure. For 2 rows, one sees 1 peak [Fig. 3(h)]; for 3 rows, one sees 2 peaks [Fig. 3(i)]; 4 rows, one sees 3 peaks [Fig. 3(j)]; 5 rows, one predicts 4 peaks [Fig. 3(k)] but the last one is out of the homogenization range, so it is strongly reduced by the diffraction of the structure.

For frequencies around $fa/c_{host} = 0.4$ we see in Fig. 3(f) that there is a deep in the diffusion coefficient produced by the presence of the band gap of the structure, due to the specular character of the reflections in the band gap as the SC behaves as a flat panel. For frequencies around $fa/c_{host} = 0.6$ a peak of diffusion is present for all the structures, whose frequency is independent of the number of columns and rows. This peak corresponds to the diffusion produced due to the impedance mismatch between the host material and the second propagating band of the SC. Moreover we see that the value of the diffusion coefficient corresponding to this peak increases as one increases the number of rows of the crystal. This is due to the fact that as the number of rows of the simulated crystal grows it approximates to the ideal case in which the structure is infinite and effects related to periodicity are enhanced.

Finally, around $fa/c_{host} \simeq 1$ we observe also a peak of the diffusion coefficient. This peak is related with the periodicity of the first row, which introduces the high diffraction orders due to the grating at the interface between the air and the SC. Particularly, this peak can be related to the well known Wood's anomalies in periodic structures [25].

In conclusion, three mechanisms can be used to reduce the direct component of the reflected wave on the specular direction considering only the diffusion produced by a SC: (*i*) the Fabry–Pérot resonances due to the finite width of the structure, (*ii*) the particular diffractive properties characteristic of the second propagating band of the SC, and (*iii*) the high diffraction orders due to the diffraction grating present at the interface between the air and the SC.

4. Experimental setup

4.1. Subscaled system and data acquisition

The experimental setup is depicted in Fig. 4. It consists of a source (ultrasonic transducer), a receiver (hydrophone) and, as we will discuss later in the Section 6, a simplified mock-up of the Vega launch pad (ZL "Zone de Lancement") at the European Space Agency's Spaceport in French Guiana [22], made of a metallic plate (iron). The experimental setup is immersed in a water tank made of Plexiglass. For practical convenience the acoustic setup is aligned horizontally with respect of the bottom of the tank without relevance in the results as gravity plays no role. The receiver is a miniature probe omnidirectional hydrophone specifically designed as a standard reference hydrophone for high frequencies, in the range [10–800] kHz. Both emitter and receiver have linear responses in the range of frequencies and amplitudes of the experiment. The dimensions of the water tank are big enough to avoid reflected waves on their walls by using the appropriate temporal

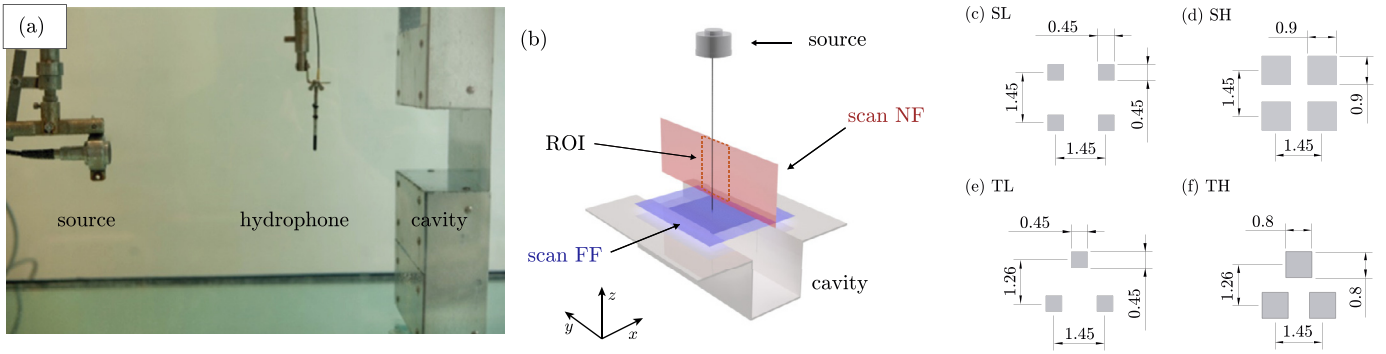

Fig. 4. (a) Photograph of the experimental setup including the acoustic source (ultrasonic transducer), the receiver (hydrophone) and the channel. (b) 3D schematic of the experimental setup. The measurement plane is represented in red and the region of interest (*ROI*), delimited by a red dashed, line used to provide spatially integrated values of the acoustic magnitudes. Lattice geometry of the four 2D SCs designed and manufactured: (c) Square lattice-Low filling fraction (SL), (d) Square lattice-High filling fraction (SH), (e) Triangular lattice-Low filling fraction (TL), (f) Triangular lattice-High filling fraction (TH). (For interpretation of the references to colour in this figure, the reader is referred to the web version of this article.)

window in the signal processing. A 3D positioning acquisition system is used to scan the measurement planes as shown in Fig. 4(b). Two planes are measured. First, a sagittal plane (y–z plane labelled as "scan NF" in Fig. 4(b)), of size 160×80 mm, which is scanned in steps of 0.5 mm. This plane is used to calculate the *IL*. A smaller centred window of 60×30 mm in this plane is the region of interest (*ROI*). It is the target region in which the noise reduction is to be obtained, and it is used to provide spatially integrated values of the *IL*. Second, a transversal area (x–y plane labelled as "scan FF" in Fig. 4(b)) of size 140×140 mm is scanned in steps of 0.5 mm, i.e., covering the SC area. This second scanned plane is used to calculate the polar scattering of the structure in the far-field by using a Fraunhofer–Fourier integration [13]. Then, the diffusion coefficient is calculated by using Eqs. (1)–(2). The acoustic magnitudes are analysed in the working frequency range [200–800] kHz.

The acoustic response on reflection of the system is evaluated in the working frequency range using the impulse response measurement technique [26]. It allows us both the separation of incident and reflected waves by windowing in the time domain and a signal-to-noise ratio that is significantly high. A sine-sweep signal frequency is generated and emitted by the transducer covering the whole working frequency range. The response signal is captured by the receiver (hydrophone) and the impulse response of the system is obtained by the convolution of the emitted signal inverted in time and the response signal experimentally measured [26].

In order to study the acoustic performance of the SCs, two different configurations have been measured:

1. SCs configuration: SCs with the scatterers aligned perpendicular to the direction of the channel, see Fig. 2(c). The backing cavity dimensions are $h = 79$ mm, $L = 100$ mm, and $L_c = 3L$.
2. Reference configuration: A flat reflector with the same dimensions as the SCs, see Fig. 2(b), used as a reference for the analysis of the reflected pressure field.

4.2. Analysed samples

Four different SC structures have been designed and manufactured as test samples for the experiments (see Figs. 4(c)–(f)). The structures are made of parallel metallic squared rods acting as sound rigid scatterers arranged in square (S) and triangular (T) lattices and with two different filling fractions (F), high (H) and low (L), leading to four combinations: Square lattice-Low filling fraction (SL, $F = 9.6\%$), Square lattice-High filling fraction (SH, $F = 39\%$), Triangular lattice-Low filling fraction (TL, $F = 11.1\%$) and Triangular lattice-High filling fraction (TH, $F = 35.1\%$). They have been fabricated in titanium using an Additive Manufacturing process known as Selective Laser Melting (SLM) [27]. Titanium has an acoustic impedance of 18.8 times the impedance of water. Therefore it could be considered as an acoustically rigid material. The samples were produced on a Concept M2 Laser Cusing Machine with a 200 W laser. Figs. 4(c)–(f) show the type of unit cells of each structure by showing a section in the plane normal to the rods. The lattice constant is the same for all the crystals: $a = 1.45$ mm. This value has been chosen to provide a band gap centred approximately at 500 kHz. The total size of all the SCs is $8 \times 100 \times 100$ mm. The rest of the dimensions are depicted in Figs. 4(c)–(f).

5. Results

5.1. Diffusion of acoustic waves by SCs

We start showing the scattering features of the SCs in the far-field. The scattered acoustic waves in the far-field provide information about the direction of the acoustic waves reflected by the structures. The scattered field is shown in Figs. 5(a)–(c) for the TL configuration and in Figs. 5(d)–(f) for the reference flat reflector, measured at three frequencies $f = 360$, 500 and 660 kHz, covering the frequency region of the FP modes, the BG frequencies and the diffractive regime respectively, i.e., the three contributions to the diffusion that we previously identified in the numerical study shown in Section 3. First, for frequencies below the BG, e.g. at 360 kHz, waves are scattered by the structure in others directions while in the specular direction the energy is reduced, as it is shown in Fig. 5(a). The SC scatters more energy in non-specular directions than the reference flat reflector, shown in Fig. 5(d). The corresponding diffusion coefficient, normalized to the diffusion coefficient of the reference flat reflector, is shown in Fig. 5(g). As the coefficient is greater than 0, the SC is efficient to spread the acoustic energy non-specularly in this frequency band. This first frequency regime corresponds to the FP resonances between the SC and the backing cavity. Second, at frequencies around the BG frequency ($\lambda \approx a/2$), i.e., around 500 kHz, waves cannot propagate through the periodic structure and energy is reflected back. The structure behaves almost as a rigid flat reflector, as shown in Fig. 5(b) and Fig. 5(e), respectively. Due the strong specular backscattering produced by Bragg interferences, a dip in the diffusion coefficient is observed. In this regime the diffusion of sound produced by the SC is of the order of the flat reflector. Note that due to the finite size of the structure (6 rows) and due to the existence of the backing cavity, not all the energy is specularly reflected and as a consequence, for the TL sample, the minimum normalized diffusion coefficient reaches a value of $\delta_n = 0.13$. Fi-

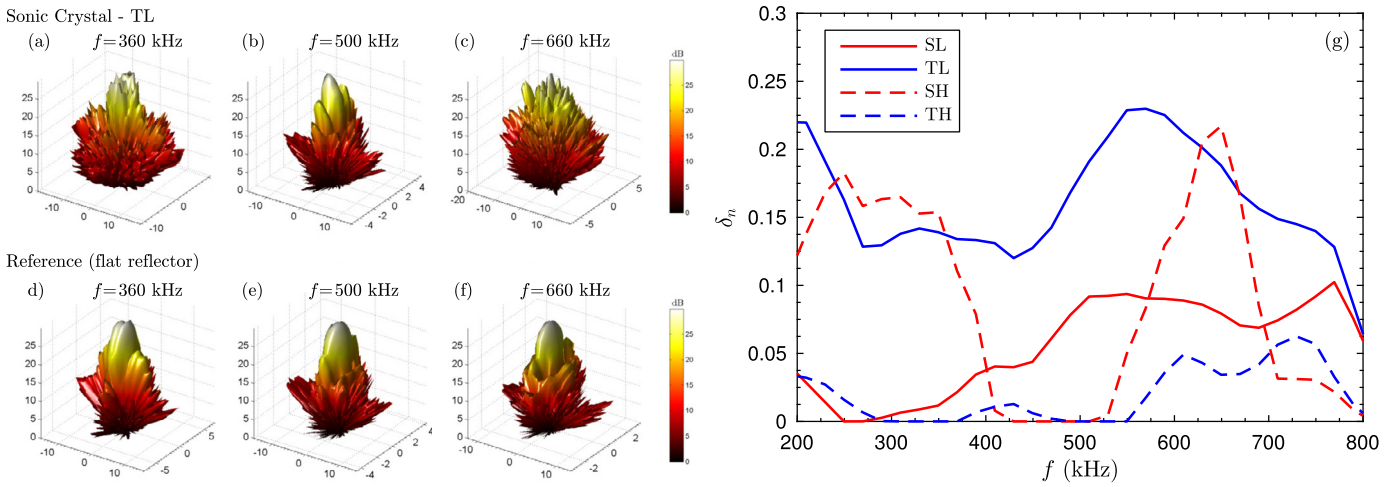

Fig. 5. (a)–(c) Scattering polar response for the sonic crystal (TL) at frequencies $f = [360, 500, 660]$ kHz respectively. Colormap in $10\log_{10}|p/p_{\max}|$. (d)–(f) Corresponding scattered field for the reference flat reflector. (g) Normalized diffusion coefficient of the four SC, δ_n, normalized to the diffusion coefficient of the reference flat reflector, δ_0. (For interpretation of the references to colour in this figure, the reader is referred to the web version of this article.)

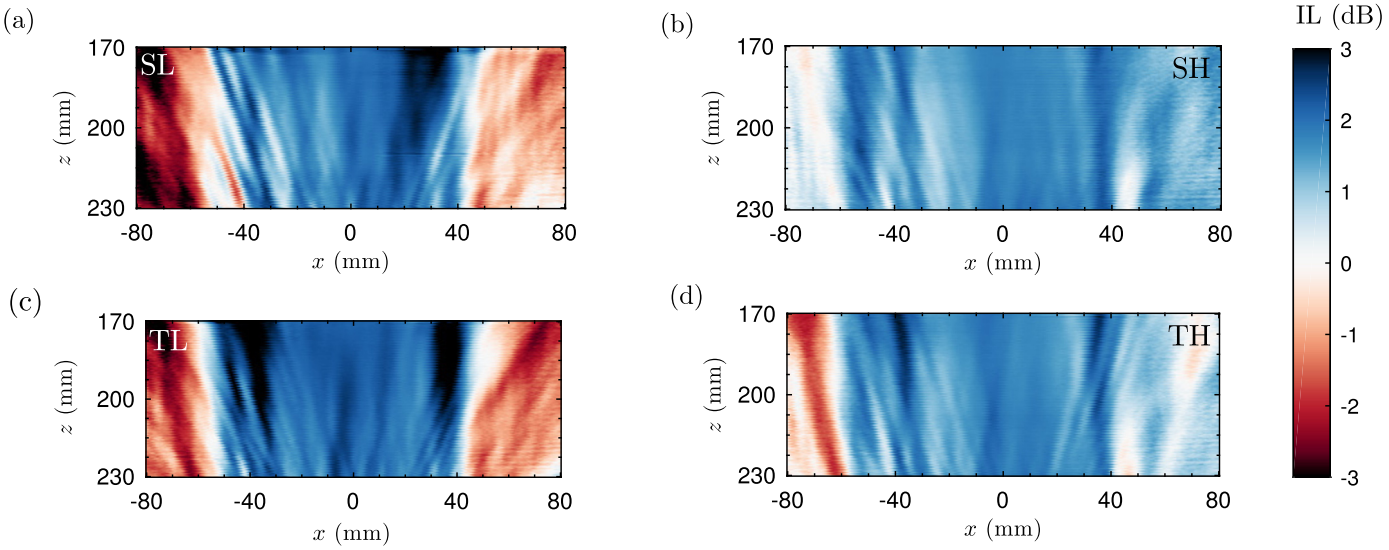

Fig. 6. Spatial distribution of the *IL* corresponding to the four SC structures tested integrated in frequency: (a) SL, (b) SH, (c) TL, (d) TH. (For interpretation of the references to colour in this figure, the reader is referred to the web version of this article.)

nally, above the BG frequency, i.e. for frequencies of about $\lambda \approx a$, waves experience strong diffraction. In this regime the scattering of acoustic waves is remarkably different from the one of a flat reflector, as it is shown in Figs. 5(c), (f) for 660 kHz. The multiple scattering between the rows that compose the SC produces a complex scattering pattern that evenly distributes the reflected acoustic energy in a broad range of directions, as it is shown in Fig. 5(c). Thus, the diffusion coefficient in this frequency regime present a peak value of $\delta_n = 0.24$ for the TL configuration.

The rest of configurations measured, SH, TH, SL, present a similar performance and their scattering properties can also be roughly divided in the three regimes previously described. The diffusion coefficient as a function of the frequency is shown in Fig. 5(g). First, for frequencies below the BG, a big difference is observed in the diffusion coefficient for the SH and TH samples. For the SH case, at normal incidence, certain part of an incident wave can travel through the crystal without facing any obstacle, while in the TH sample, due to the geometry of the unit cell, any part of the incident wave will be able to propagate through the crystal without facing any obstacle (see the geometry of the unit cells in Figs. 4(d), (f)). Hence, the TH sample reflects a big part of the incident wave, despite being at frequencies below the BG, while the SH sample allows the wave to pass through and the dispersion effects of the crystal arise, resulting in much higher values of the diffusion coefficient. In order to compare the effect of the filling fraction, we describe the results between the same kind of unit cell, describing the square lattice samples, SL, SH. For the former, the system is mostly transparent and the reflected wave comes mostly from the bottom of the cavity, which is a flat surface, producing a very small value of the diffusion coefficient. While for the latter, as mentioned previously, dispersion effects are playing their role in a much more intensive manner. Multiple internal non-specular reflections are caused between the SCs and the cavity due to the anisotropic propagation in the SCs. Thus, the directions of the waves when they come out of the structure are tilted in a broad range of angles, increasing the value of the normalized diffusion coefficient. At BG frequencies all the structures present a dip in the diffusion caused by the Bragg interferences: the energy inside the cavity is reduced and waves are reflected in a quasi-specular manner. The dip in the frequency-dependent diffusion produced by the BG is more pronounced for SCs having higher filling fractions, as the SH (dashed red curve in Fig. 5(g)).

Finally, at higher frequencies, in the diffractive frequency regime, the multiple scattering between the rods increases the complexity in the propagation: the strongly anisotropic propagation inside the SC produces a scattering pattern which is more omnidirectional than the reference flat reflector. Again, structures with lower filling fraction present more uniform scattering patterns, i.e, higher diffusion coefficients. In particular, the TL sample presents the highest value of the diffusion coefficient and the best frequency broadband behaviour of all SCs analysed in this work.

5.2. Noise reduction of the specular waves around the sound source location (near field)

The situation in the near field is analysed here. For that purpose, the *IL* in reflection, as introduced in Subsection 2.2.2, is used. Fig. 6 shows the spatial distribution of *IL* integrated in frequency for all the SCs experimentally tested. Each point represents the value of *IL* integrated in the working frequency range, [200–800] kHz. It is worth noting here that the measured area shown in the four insets of Fig. 6 corresponds precisely to the red rectangle shown in the 3D schematic of the experimental setup (see Fig. 4(b)). Moreover, lower z values represent points located closer to the acoustic source, while higher z values represent points closer to the SC (the origin of coordinates is located in the centre of the radiating surface of the ultrasonic transducer, as shown in Fig. 4(b)). Positive values plotted in blue correspond to measurement points in which the total field in the configuration with the SC sample is lower than the total field of the reference configuration. As a consequence, the SC scatters waves through other directions rather than the specular one and a noise reduction is produced. On the contrary, for areas in red *IL* values are negative and the sound pressure level, in the configuration with the SC, is higher than that of the reference configuration. It is observed that the central region of the measurement area is predominantly blue for all the SCs tested, especially in the region corresponding to the *ROI* (see Fig. 4(b)). It is noticed that an asymmetry in the spatial distribution of the *IL* for all the four samples is observed. This is due to a small misalignment of the samples with respect to the x–y plane. These results indicate that, due to the particular scattering properties of the SCs, there is an important spatial spreading of the acoustic energy in the near field of the SCs. Moreover, it is clearly observed how the SCs having lower filling fraction present higher dispersion, especially in the case of the triangular unit cell and low filling fraction (TL), as shown in Fig. 6(c). A more detailed description of the influence of the filling fraction requires the analysis of particular frequency ranges and it is presented below.

A different analysis of the experimental results is performed evaluating the spatial integration in the *ROI* of the *IL*, showing in this case the variation in frequency. In Fig. 7 grey bars represent the *IL* integrated over the *ROI* in frequency bands, and the red bar shows the overall value of the *IL* integrated both in space and frequency. A common pattern for all structures is that they present lower values of *IL* at frequencies in the band gap (around 500 kHz). However, following the same trend observed previously in the case of the diffusion coefficient, at frequencies laying in the BG, structures with higher filling fraction manifest more clearly the specular character of the reflection. To further illustrate these differences between the reflection produced at BG frequencies, Supplementary Videos 1 and 2 showing the propagation and reflection of a burst sinusoidal signal composed of 8 cycles and frequency $f = 500$ kHz are provided for two of the tested samples, SH [28], and TL [29]. For both cases, the videos show the comparison of a travelling pulse reflecting at the SC and the same pulse reflecting at the reference flat reflector. The reflection caused by the sample SH is very similar to the reference flat reflector, i.e., specular, causing a minimum value of the *IL* (see Fig. 7(b)). On the contrary, the low filling fraction of the sample TL, combined with its finite size, reduces the manifestation of the BG effects, causing a less specular reflection, resulting in higher values of the *IL* at that frequency in the *ROI* (see Fig. 7(c)). For frequencies above the BG, corresponding to the second propagative band of the triangular lattice SCs, a strong non-specular reflection is observed, resulting in high *IL* values (see frequencies above 600 kHz in Figs. 7(c), (d), for instance). However, for the SCs with the square lattice, the *IL* at these frequencies decreases due to the spatial filtering effect [30] (see frequencies above 600 kHz in Figs. 7(a), (b)). Supplementary Video 3 shows the non-specular reflection caused by a burst sinusoidal signal composed of 8 cycles at a frequency $f = 650$ kHz, which corresponds to the second propagating band of the crystal, impinging the sample TL, in comparison to the reflection at the reference flat reflector [31]. Globally, results presented in Fig. 7 show that the filling fraction has more influence than the type of unit cell in the *IL*; the highest *IL* values are found for the structures with low filling fraction, being the type of unit cell not so relevant. A *IL* value of around 2 dB is observed for all the samples. Finally, the highest acoustic field reduction among the analysed configurations ($IL = 2.2$ dB) is achieved by the SC with low filling fraction and triangular lattice (TL).

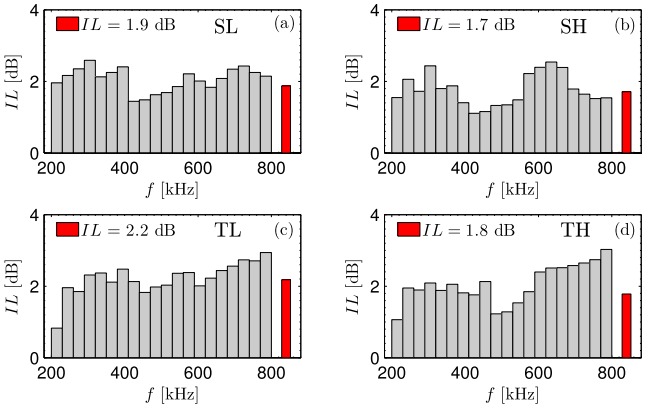

Fig. 7. *IL* integrated in the ROI with the four SC structures tested: (a) SL, (b) SH, (c) TL, (d) TH. The inset of the red bar represents the *IL* value integrated in space (*ROI*) and frequency ([200, 800] kHz). (For interpretation of the references to colour in this figure, the reader is referred to the web version of this article.)

6. Discussion for aerospace applications

The launch of rockets or space shuttles is an extreme event, in which the involved physical conditions (temperature, gas flow, pressure) exceed those in conventional situations by orders of magnitude [32]. In particular, the exhaust plume from a rocket engine generates severe acoustic waves, which cause acoustic and vibration loading on the ground structures and vehicle payload. Unlike other physical processes involved at the launch site, the acoustic environment and the noise level control at the launch site has received much less attention since the design is primarily focused on solving two other important problems: channelling of exhaust gases and withstanding extreme heat. However, the acoustic loads experienced by the launch vehicle occur with strong interaction between the rocket and the launch facility, therefore putting at risk the mission with potentially high economic cost. Thus, the prediction and reduction of the acoustic levels in the near field of the launch vehicle is an important factor that should be taken into consideration early in the design process of the space launch complex. Recent studies show the relevance of the noise reduction problem in the launch pad, since it is predicted to improve the reliability and operations of future launchers [15–19].

During the lift-off, the airborne sound generated by the exhaust stream of the rocket engine can be separated in its direct component (radiating directly from the flame deflector) and the reflected one due to the interaction of the sound waves with both the flame deflector and the launch pad structures. Both components can be transmitted into the interior of the rocket mainly via re-radiation from the vibrating walls. There is considerable literature predicting and proposing technologies for the mitigation of aircraft noise [33,34]. Some strategies act inside the fairing by using dampers, [35–37] or by using active materials [38,39] with the main objective of reducing the structure borne noise in the rocket [40–45]. Others act externally, at the level of the launch pad, in order to reduce both the direct and the reflected components of the airborne sound. The most commonly applied is the injection of pressurised water flow [46–52]. This consists of water jets released by systems installed on the pads, with the purpose of absorbing enough sound to reduce the direct component of the jet noise, achieving levels just below the design requirements. Others mechanisms are based on the optimisation of the shape of the flame deflector in order to reduce the back reflected component of the airborne sound waves [20,21]. In this work we presented a proof of concept to reduce the reflected acoustic energy by using SCs placed over a cavity. The motivation of this work was the first attempt to develop large-scale passive structures to reduce the reflected acoustic energy for aerospace applications. In particular, the analysed samples were designed with a scale factor of 1:60 with respect to the Vega launch pad (ZL "Zone de Lancement") at the European Space Agency's Spaceport in French Guiana [22], operated by Arianespace SA. In the real-world scale, the SCs are made by 6×70 metal beams of $L_{RW} = 6$ m length separated periodically $a_{RW} = 8.7$ cm, each one of $l_{RW} = 4.8$ cm thickness for TH and SH samples ($l_{RW} = 2.7$ cm for TL and SL samples). The cavity, of $L_{RW} = 6$ m width and $h_{RW} = 4.2$ m height, corresponds to a minimal-complexity scaled model of the exhaust-gas duct of the Vega ZL, see Ref. [22] for further details. This gives a frequency scaling factor of 1:250, being the frequency range studied covering from 800 to 3200 Hz. It is worth noting here that a smaller scale model will allow to study a lower frequency regime, e.g. from 250 to 500 Hz, but this was out of the available precision for the titanium 3D printing machine. On the other hand, water was selected as the host fluid to maintain the scale of the thermoviscous losses inside the SC: the current scaling provides a ratio of 1:1.08 between the ratio of the viscous boundary-layer length and the lattice step in the real-scale problem (air) and in the corresponding one in the scale-model (water). Note the corresponding scaling in air would lead to visco-thermal losses more than one order of magnitude bigger then in the scale model with respect to the real-scale problem and, therefore, the *IL* performance would be overestimated due to acoustic absorption.

Although this proof of concept allows to understand the reflection characteristics of the SCs and to prove the deflection of sound in non-specular directions, the considered problem is greatly simplified and there are some important factors in the experimental conditions that are far from the real conditions in the launchpad. Hence, they should be taken into account in future studies, including: (*i*) In the current experiments, the acoustic source was a highly directive beam placed over the top of the cavity, while during the launch, the aeroacoustic source of noise is spatially distributed along the hot gases from the engine plume and also inside the exhaust-gas ducts [53]. (*ii*) The frequency content of the incident field used in the experiments was limited to two octave bands. (*iii*) The vibro-acoustic coupling between the host fluid and the metal beams that composes the SCs is stronger in water than in air. However, note that during launch water deluge systems can be combined with SCs, improving the vibro-acoustic coupling between the host fluid and the SCs scatterers. (*iv*) The extreme amplitude of the acoustic waves during the lift-off involves highly nonlinear acoustic propagation and turbulent fluids with extreme pressure, density and temperature gradients. All these important factors imply that, once the first proof of concept has been realized in this scale model, further experimental tests under more realistic conditions are to be performed in order to validate experimentally SCs in a real-scale situation as a solution to deflect acoustic energy and reduce acoustic loading during lift-off.

7. Conclusions

The reflection performance of Sonic Crystals (SC) has been presented numerically and experimentally. The reduction of the reflected energy and the diffusion coefficients of four SCs with different unit cells and filling fractions have been measured in a water tank in a scale-model and in the ultrasonic regime. Under these conditions, the main effect of the SCs is to distribute the acoustic energy evenly in space: The measured diffusion coefficient reaches values of 0.25, while the *IL* is close to 2 dB in a frequency band covering two octaves. This represents a decrease of the 37% of the acoustic energy in front of the structures.

The results show that SCs can reduce broadband noise levels at the location of an acoustic source due to the reduction of the specular reflection and the deflection of acoustic waves in other directions. The fact that the SCs are structured and inhomogeneous media, as well as the propagation inside them is strongly dispersive and anisotropic, is at the root of the non-specular reflection, mainly responsible to the noise reduction mechanism shown here.

The proof of concept presented here is the first attempt to apply SCs as a solution to reduce the acoustic load during the lift-off of launch vehicles for aerospace applications. The placement of SCs on the top of the channel for exhausting gases can remove energy in the region where the launcher is placed, acting on the sound waves that are reflected by the launchpad. Although SCs are revealed as a feasible solution to be explored for noise mitigation at launchpads, its behaviour for sound damping can be strongly improved including other effects like local resonances or by optimizing the geometry of the SCs to maximize the viscothermal and viscoelastic losses. Moreover, SCs are open structures that allow the pass of fluids, therefore there are compatible with other damping mechanisms already used in the launch pads as water deluge systems. However, due to the extreme complexity of the problem and the limitations of the scale-model presented, further experimental research in experimental conditions closer to the real-scale situation is needed.

Conflict of interest statement

None declared.

Acknowledgements

We want to thank Julian Santiago-Prowald (ESA) and Vicente Gomez Molinero (formerly at Airbus D&S) for fruitful discussions. Authors acknowledge the support of the European Space Agency under contract "Sonic Crystals For Noise Reduction At The Launch Pad", ESA ITT 1-7094 (ITI) and the 441-2015 Co-Sponsored PhD "Acoustic Reduction Methods for the Launch Pad". The work was supported by Spanish Ministry of Economy and Innovation (MINECO) and European Union FEDER through project FIS2015-65998-C2-1 and FIS2015-65998-C2-2.

Appendix A. Supplementary material

Supplementary material related to this article can be found online at https://doi.org/10.1016/j.ast.2017.11.048.

References

[1] R. Martínez-Sala, J. Sancho, J.V. Sánchez, V. Gómez, J. Llinares, F. Meseguer, Sound attenuation by sculpture, Nature 378 (6554) (1995) 241.
[2] J.V. Sánchez-Pérez, D. Caballero, R. Martínez-Sala, C. Rubio, J. Sánchez-Dehesa, F. Meseguer, J. Llinares, F. Gálvez, Sound attenuation by a two-dimensional array of rigid cylinders, Phys. Rev. Lett. 80 (24) (1998) 5325–5328.
[3] J.V. Sánchez-Pérez, C. Rubio, R. Martínez-Sala, R. Sánchez-Grandia, V. Gómez, Acoustic barriers based on periodic arrays of scatterers, Appl. Phys. Lett. 81 (27) (2002) 5240–5242.
[4] V. Romero-García, C. Lagarrigue, J.-P. Groby, O. Richoux, V. Tournat, Tunability of band gaps and waveguides in periodic arrays of square-rod scatterers: theory and experimental realization, J. Phys. D, Appl. Phys. 46 (2013) 305108.
[5] V. Romero-García, J.V. Sánchez-Pérez, S. Castineira-Ibánez, L.M. Garcia-Raffi, Evidences of evanescent bloch waves in phononic crystals, Appl. Phys. Lett. 96 (12) (2010) 124102.
[6] A. Cebrecos, V. Romero-García, R. Picó, I. Pérez-Arjona, V. Espinosa, V. Sánchez-Morcillo, K. Staliunas, Formation of collimated sound beams by three-dimensional sonic crystals, J. Appl. Phys. 111 (10) (2012) 104910.
[7] V. Romero-García, J.V.S. Pérez, L.M.G. Raffi, Tunable wideband bandstop acoustic filter based on two-dimensional multiphysical phenomena periodic systems, J. Appl. Phys. 110 (2011) 149041.
[8] V. Romero-García, A. Cebrecos, R. Picó, V.J. Sánchez-Morcillo, L.M. Garcia-Raffi, J.V. Sánchez-Pérez, Wave focusing using symmetry matching in axisymmetric acoustic gradient index lenses, Appl. Phys. Lett. 103 (2013) 264106.
[9] I. Pérez-Arjona, V.J. Sánchez-Morcillo, J. Redondo, V. Espinosa, K. Staliunas, Theoretical prediction of the nondiffractive propagation of sonic waves through periodic acoustic media, Phys. Rev. B 75 (2007) 014304.
[10] V. Sánchez-Morcillo, R. Picó, I. Pérez-Arjona, K. Staliunas, Spatial filtering of sound beams by sonic crystals, Appl. Acoust. 73 (2012) 302.
[11] M. Sigalas, Elastic wave band gaps and defect states in two-dimensional composites, J. Acoust. Soc. Am. 101 (1997) 1256.
[12] J. Redondo, R. Picó, V.J. Sánchez-Morcillo, W. Woszczyk, Sound diffusers based on sonic crystals, J. Acoust. Soc. Am. 134 (6) (2013) 4412–4417.
[13] T.J. Cox, P. D'antonio, Acoustic Absorbers and Diffusers: Theory, Design and Application, CRC Press, 2009.
[14] Sonic Crystals for Noise Reduction at the Launch Pad, Tech. Rep., European Space Agency under Contract ITT 1-7094 (ITI) 2014.
[15] D. Gély, G. Elias, F. Mascanzoni, H. Foulon, Acoustic environment of the vega launch vehicle at lift-off, in: Proceedings of the Forum Acusticum, Budapest, 2005.
[16] G. Elias, Ariane 5 at lift off: localization and ranking of acoustic sources, in: 29th International Congress and Exhibition on Noise Control Engineering. Internoise 200, 2000, pp. 1–7.
[17] J. West, L.L. Strutzenberg, Development of modeling capabilities for launch pad acoustics and ignition transient environment prediction, in: Proceedings of the 18th AIAA/CEAS Aeroacoustics Meeting Conference, 2012.
[18] R. Venkatraman, S. Sankaran, S.V. Subba Rao, P. Krishnaiah, T. Sundararajan, Investigation on the ignition over pressure related to launch vehicle lift-off, Indian J. Sci. Technol. 71 (1) (2014) 86–94.
[19] A. Vorobyov, T. Abdurashidov, V. Bakulev, A. But, A. Kuznetsov, A. Makaveev, Problem of intensity reduction of acoustic fields generated by gas-dynamic jets of motors of the rocket-launch vehicles at launch, Acta Astronaut. 109 (2015) 264–268.
[20] S. Tsutsumi, S. Kato, K. Fukuda, R. Takaki, K. Ui, Effect of deflector shape on acoustic field of launch, in: 47th AIAA Aerospace Sciences Meeting, Orlando, Florida, 5–8 January, 2009, pp. 1–8.
[21] S. Tsutsumi, T. Ishii, K. Ui, S. Tokudome, K. Wada, Study on acoustic prediction and reduction of epsilon launch vehicle at liftoff, J. Spacecr. Rockets 52 (2) (2015) 350–361.
[22] Arianespace, Vega user's manual, issue 4 – revision 0 (April 2014), http://www.arianespace.com/publication/vega-users-manual/.
[23] R.P. Moiseyenko, S. Herbison, N.F. Declercq, V. Laude, Phononic crystal diffraction gratings, J. Appl. Phys. 111 (2012) 034907, https://doi.org/10.1063/1.3682113.
[24] D. Torrent, J. Sánchez-Dehesa, Effective parameters of clusters of cylinders embedded in a nonviscous fluid or gas, Phys. Rev. B 74 (2006) 224305.
[25] V.M. García-Chocano, J. Sánchez-Dehesa, Anomalous sound absorption in lattices of cylindrical perforated shells, Appl. Phys. Lett. 106 (2015) 124104.
[26] A. Farina, Simultaneous measurement of impulse response and distortion with a swept-sine technique, in: Proc. AES 108th Conv., Paris, France (I), 2000, pp. 1–15.
[27] C. Qiu, N. Adkins, M. Attallah, Microstructure and tensile properties of selectively laser-melted and of HIPed laser-melted Ti–6Al–4V, Mater. Sci. Eng. A 578 (2013) 230–239.
[28] See supplementary video 1 travelling-pulse-sh-500 kHz at journal link.
[29] See supplementary video 2 travelling-pulse-tl-500 kHz at journal link.
[30] V. Romero-García, R. Picó, A. Cebrecos, K. Staliunas, V. Sánchez-Morcillo, Angular band gaps in sonic crystals: evanescent waves and spatial complex dispersion relation, Vib. Acoust. 135 (4) (2013) 041012.
[31] See supplementary video 3 travelling-pulse-tl-650 kHz at journal link.
[32] J.P. Arenas, R.N. Margasahayam, Noise and vibration of spacecraft structures, Rev. Chil. Acust. 14 (3) (2006) 251–264.
[33] D. Casalino, F. Diozzi, R. Sannino, A. Paonessa, Aircraft noise reduction technologies: a bibliographic review, Aerosp. Sci. Technol. 12 (1) (2008) 1–17.
[34] W. Dobrzynski, R. Ewert, M. Pott-Pollenske, M. Herr, J. Delfs, Research at DLR towards airframe noise prediction and reduction, Aerosp. Sci. Technol. 12 (1) (2008) 80–90.
[35] C.H. Sohn, J.H. Park, A comparative study on acoustic damping induced by half-wave, quarter-wave, and Helmholtz resonators, Aerosp. Sci. Technol. 15 (8) (2011) 606–614.
[36] S.A. Lane, K. Henderson, A. Williams, E. Ardelean, Chamber core structures for fairing acoustic mitigation, J. Spacecr. Rockets 44 (1) (2007) 156–163.
[37] G. Ghiringhelli, M. Terraneo, E. Vigoni, Improvement of structures vibroacoustics by widespread embodiment of viscoelastic materials, Aerosp. Sci. Technol. 28 (1) (2013) 227–241.
[38] A. Grewal, D. Zimcik, B. Leigh, Feedforward piezoelectric structural control: an application to aircraft cabin noise reduction, J. Aircr. 38 (1) (2001) 164–173.
[39] T. Bein, J. Bös, S. Herold, D. Mayer, T. Melz, M. Thomaier, Smart interfaces and semi-active vibration absorber for noise reduction in vehicle structures, Aerosp. Sci. Technol. 12 (1) (2008) 62–73.
[40] R.E. Caimi, R.N. Margashayam, J.F. Nayfeh, Launch-Induced Vibration and Ignition Overpressure Response, Tech. Rep., 2001.
[41] F. Mastroddi, G. Coppotelli, G.M. Polli, C.D.I. Trapani, Vibro-acoustic response analysis to pressure oscillations in a solid rocket motor – comparisons with the experimental fire-test data, in: Aerotecnica Missile e Spazio, vol. 86, 2007, p. 109.
[42] M. Morshed, M. Maruf, Investigation of External Acoustic Loadings on a Launch Vehicle Fairing During Lift-off Mir Md. Maruf Morshed, Ph.D. thesis, 2008.
[43] H. Park, H. Seo, K. Jeong, S. Jang, M. Yi, R. Cho, Lift-off vibro-acoustic analysis of the upper stage of small launch vehicle, in: Proceedings of the 13th International Congress on Sound and Vibration, 2006, pp. 2–9.
[44] R. Pirk, A. Souto, G.P. Guimaraes, L. Carlos, S. Góes, Acoustics and vibroacoustics applied in space industry, in: Modeling and Measurement Methods for Acoustic Waves and for Acoustic Microdevices, 2013, pp. 479–512, Ch. 20.
[45] D. Saravanan, C. Lakshmana Dora, T. Murugan, S. Sankaran, T. Satyanarayana, D. Das, Experimental investigation of flow and noise characteristics of impinging twin jets, simulating starting flow from a rocket booster on a launch pad, in: National Conference on Space Transportation Systems: Opportunities and Challenges, no. October 2015, 2011.
[46] Y. Marchesse, Y. Gervais, H. Foulon, Water injection effects on hot supersonic jet noise, C. R., Méc. 330 (1) (2002) 1–8.
[47] S. Sankaran, J.K. Ignatius, R. Ramkumar, T.N.V. Satyanarayana, S.R. Chakravarthy, N.R. Panchapakesan, Suppression of high mach number rocket jet noise by water injection, J. Spacecr. Rockets 46 (6) (2009) 1164.
[48] J.K. Ignatius, S. Sankaran, S.R. Chakravarthy, Supersonic jet noise and suppression characteristics during launch vehicle liftoff hot …, in: Proceedings of the 13th Asian Congress of Fluid Mechanics, Dhaka, Bangladesh, vol. 3, 2010, pp. 569–572.
[49] M. Kandula, A. Aerospace, N. Kennedy, Prediction of turbulent jet mixing noise reduction by water injection, AIAA J. 46 (11) (2008) 2714–2722.
[50] M. Kandula, Broadband shock noise reduction in turbulent jets by water injection, Appl. Acoust. 70 (7) (2009) 1009–1014.
[51] M. Kandula, Sound radiation from a supersonic jet passing through a partially open exhaust duct, J. Vib. Acoust. 133 (2011) 064503.
[52] A. Krothapalli, L. Venkatakrishnan, L. Lourenco, B. Greska, R. Elavarasan, Turbulence and noise suppression of a high-speed jet by water injection, J. Fluid Mech. 491 (2003) 131–159.
[53] J. Panda, R.N. Mosher, B.J. Porter, Identification of Noise Sources Rocket Engine Test Firings and a Rocket Launch Using a Microphone-Array, Technical Report NASA/TM-2013-216625 – ID:20140011422, NASA, 2013, http://hdl.handle.net/2060/20140011422.